19 Laser-Induced Phase Transitions in GaAs

Y. Siegal, E. N. Glezer, E. Mazur

19.1 Introduction

For over two decades the subject of laser-induced phase transitions in semiconductors has generated considerable interest. This field arose originally in the context of semiconductor annealing, a technologically important process aimed at repairing the damage to semiconductor crystals caused by dopant atom implantation. The conventional method for this process is thermal annealing – the slow baking of a semiconductor in an oven. In the heated sample the increased mobility allows defects and dislocations to diffuse to the surface. In the 1970s, a similar effect was produced by irradiating a doped semiconductor with a short laser pulse [1]. Although laser annealing of semiconductors has not replaced thermal annealing in industrial semiconductor processing, the discovery of laser annealing opened up a new and exciting chapter in the study of light-matter interactions: the use of light to alter the structure of matter.

19.1.1 Chemical Bonds and Energy Bands

The study of laser-induced structural change in semiconductor crystals lies at the intersection of chemistry and solid-state physics. This area of research highlights the intimate connection between the chemical bonds which hold a crystal together and the energy bands which describe the electronic properties of the crystal. The bond picture and the band picture are two complementary ways of looking at a solid, and although one may be more appropriate than the other for a particular discussion, an understanding of both pictures provides additional insight into crystal cohesion, electronic behavior, and laser-solid interactions.

Most of the work on laser-induced structural change has focused on Group IV and III-V semiconductors in the diamond and zinc blende crystal structures. These materials are very appropriate for studying cohesion because of the central role played by covalent bonds in their crystals. Both the diamond and the zinc blende structures are built from tetragonally coordinated atoms, with each pair of nearest neighbors held together by sharing two electrons. If a significant fraction of these

bonding electrons are excited to antibonding states, the cohesion of the crystal will be strongly affected [2]. In this chapter we focus on the removal of bonding electrons by photons from an incident laser pulse. To understand the material response to laser excitation, we should first examine the relationship between chemical bonds and energy bands.

Figure 19.1 (a) illustrates schematically a covalent bond between two atoms. If two atoms get close enough to each other so that the atomic orbitals of a particular energy level in each atom overlap, then the wavefunctions of these orbitals can add with either the same or opposite phase. This results in a splitting of the energy level of the overlapping orbitals. The lower level corresponds to the wavefunctions adding in phase, while the upper level corresponds to adding with opposite phase. If both of the original electronic levels in each atom were singly occupied (note that each

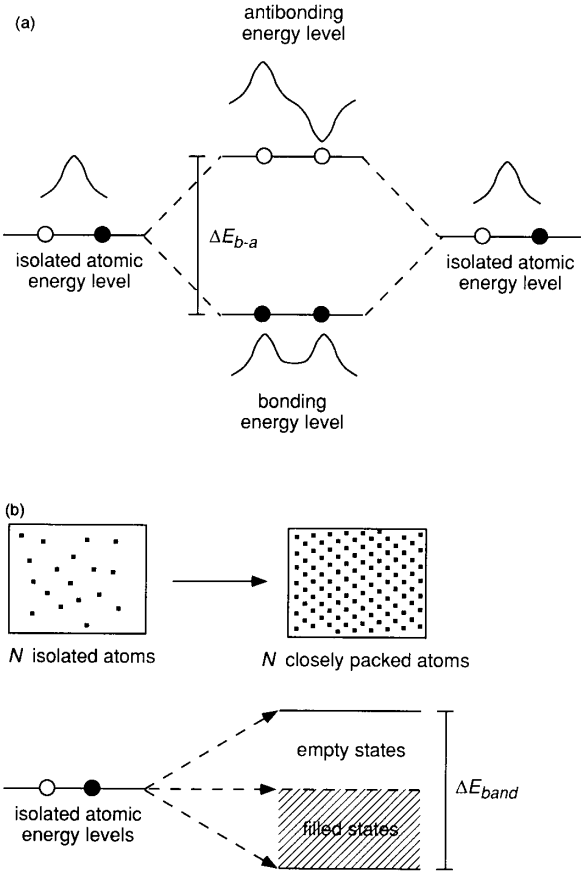

Figure 19.1 (a) Covalent bonding results from the splitting of an atomic energy level into bonding and antibonding levels separated by an energy ΔE_{b-a}. (b) Metallic bonding results from the broadening of an atomic energy level into a band of energies of width ΔE_{band}: •, filled electronic state; o, empty electronic state.

level has two spin states), then in the ground state of the new system the two electrons will occupy the lower level, which is lower in energy than the original level. Since this state is energetically more favorable than the state in which the two atoms are separated, the sharing of the two electrons results in a bond between the two atoms. However, if one or both of the electrons is excited to the upper level, then the new state no longer has a lower total energy than the state with two separated atoms. Thus, the lower level corresponds to a bonding state while the upper level corresponds to an antibonding state.

Metallic bonding arises from a more delocalized overlap of atomic orbitals in a solid. This overlap of the orbitals of a particular atomic energy level leads to a broadening of this energy level into a band of energies. If the atomic energy levels are not fully occupied (note again that each level has two spin states), then as the atoms are brought closer together to form a solid, the total energy will be lower than for the isolated atoms, as illustrated schematically in Fig. 19.1 (b). Because this type of bonding results in a partially filled energy band, such a material will exhibit metallic electronic characteristics [3].

Semiconductors exhibit characteristics of both covalent bonding and metallic bonding. On the one hand, nearest neighbors form covalent bonds by sharing two electrons, resulting in a splitting of atomic levels into bonding and antibonding states. On the other hand, these bonding and antibonding states are broadened into

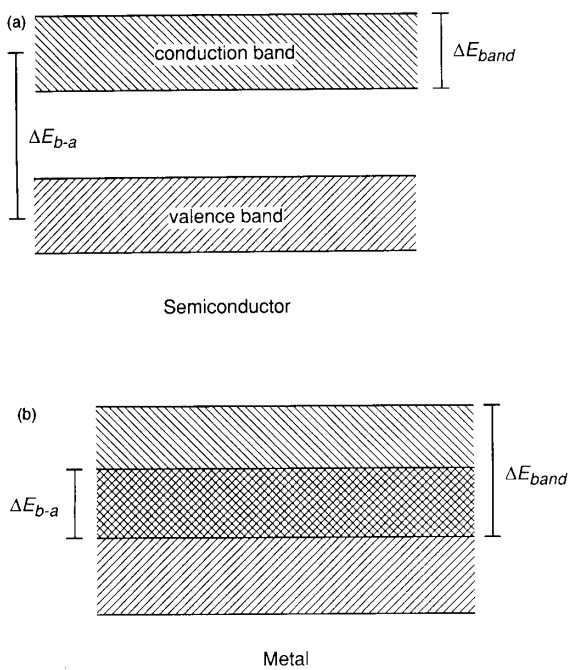

Figure 19.2 (a) Schematic representation of a semiconductor: $\Delta E_{b-a} > \Delta E_{band}$. (b) Schematic representation of a metal: $\Delta E_{b-a} < \Delta E_{band}$.

bonding and antibonding energy bands by more delocalized interactions with the other atoms in the solid. When the average bonding-antibonding splitting in the material is larger than the width of the energy bands, an energy gap will exist between the bonding and the antibonding bands (see Fig. 19.2a). If the atomic orbitals start out half-filled, then the ground state consists of a fully occupied bonding band and an empty antibonding band. In this case the material will not conduct electricity. However, when the average bonding-antibonding splitting is smaller than the width of the energy bands, the bonding and antibonding bands overlap (see Fig. 19.2b). The resulting partially filled bands lead to metallic electronic characteristics even in the ground state. A semiconductor corresponds to the former case: an energy band gap separates the bonding (valence) and antibonding (conduction) bands. While semiconductors are insulators in the ground state, they start conducting when electrons are excited from the valence to the conduction band. Conductivity in a semiconductor is mediated both by the negatively charged electrons excited to the conduction band, and by the positive holes left behind in the valence band by the excited electrons. The conducting electrons and holes are often referred to collectively as free charge carriers, or simply free carriers.

19.1.2 Previous Work

The strong connection between the electronic system and the lattice structure of a solid suggests that a change in one affects the other. When a laser pulse is incident on a semiconductor, it interacts with the electronic system in the material by exciting electrons from the valence band to the conduction band. If strong enough, this electronic excitation eventually leads to a structural change in the lattice. The central question to address then is how the excitation of the electronic system results in atomic motion.

19.1.2.1 Thermal Model versus Plasma Model

Following the first experiments in laser annealing, two models were proposed to explain the structural change resulting from electronic excitation. One, known as the thermal model, describes the structural change as a thermal melting process [4–6]. The thermal model assumes that the excited electronic system rapidly equilibrates with the lattice by exciting lattice vibrations (emitting phonons). With this assumption, the laser energy deposited in the material can be treated as though it is instantly converted to heat. If the incident laser pulse is strong enough, the irradiated part of the sample will heat up to the melting temperature and undergo a transition to the liquid phase as the latent heat of fusion is supplied.

The other model, known as the plasma model, attributes the structural change to destabilization of the covalent bonds resulting directly from the electronic excitation [7, 8]. The plasma model assumes a slower rate of phonon emission by the excited electronic system. This assumption implies that structural change can occur while

the electronic system and the lattice are not in thermal equilibrium with each other, although each of these systems may be internally in a quasiequilibrium. According to this model, the structural change is driven directly by the excited electronic system. If a sufficiently high fraction of the valence electrons are excited from bonding states to antibonding states, then the covalent bonds can no longer hold the crystal together, and a structural transition occurs.

19.1.2.2 Picosecond Pulses versus Femtosecond Pulses

The dispute over the explanation for laser-induced structural change sparked a flurry of experimental activity to test these two models. Early results, from experiments involving laser pulses with pulse widths of tens of picoseconds or longer, showed evidence for strong heating of the sample and agreed well with predictions from computer simulations based on the thermal model [4]. Later, Raman spectroscopy experiments on semiconductors confirmed that an excited electronic system can equilibrate with the lattice in just a few picoseconds [9], in agreement with the assumption in the thermal model.

The introduction of femtosecond lasers in the mid-1980s led to renewed interest in this topic [10]. The development of laser pulses with pulse widths below 100 fs opened up the possibility of depositing energy in a semiconductor on a timescale which is short compared with the electron–lattice equilibration time of a few picoseconds. Furthermore, higher densities of excited electrons than ever before could now be created because nonlinear absorption becomes important with the high peak intensities in femtosecond pulses [11]. Thus, femtosecond laser excitation of semiconductors seems to satisfy the necessary conditions for electronically driven structural change as described by the plasma model. Indeed, recent experimental results show that the response of a semiconductor to a femtosecond laser pulse is fundamentally different from its response to a picosecond or nanosecond laser pulse [10, 12–16].

19.2 Experimental Probes

Most of the experiments on laser-induced structural change involve a pump laser pulse to excite the material and a probe laser pulse to determine the response of the material to the excitation. Varying the time delay between the arrival of the pump pulse and the arrival of the probe pulse on the sample maps out the time evolution of this response. Because the photons in both the pump pulse and the probe pulse couple directly to the electronic system, not to the lattice, these experiments involve the connection between energy bands and chemical bonds in two ways: in causing the structural change and in characterizing it. First, by altering the electronic distribution within the energy bands, the pump pulse induces a change in the chemical bond structure. Then, by monitoring changes in the electronic response to

light, the probe pulse provides information on how the chemical bond structure changes following the excitation. This section explores some of the specific techniques used to extract information on the chemical bond structure using an optical probe.

19.2.1 Reflectivity

Using the probe pulse to measure the reflectivity for a particular polarization and angle of incidence constitutes the simplest optical probe. While its measurement is a relatively simple operation, the reflectivity does not provide direct information on the electronic band structure. The reflectivity is related to the dielectric constant, which, in turn, is determined by the electronic band structure. In general, since the dielectric constant has both a real part and an imaginary part, a reflectivity measurement at a single polarization and angle of incidence is insufficient to determine material properties uniquely.

However, when the real and imaginary parts of the dielectric constant can be modeled by a single parameter, the reflectivity provides enough information to extract the dielectric constant. A single-parameter model that is used extensively for optically excited semiconductors is a modified Drude model [5, 17]. The basic Drude model describes the response of free electrons to light [3]. In the modified version the dielectric constant of the semiconductor is

$$\varepsilon(\omega) = 1 + 4\pi\chi_{\text{interband}}(\omega) + 4\pi\chi_{\text{Drude}}(\omega) \tag{1}$$

where ω is the angular frequency of the incident light. The term $\chi_{\text{interband}}(\omega)$ describes the contribution of interband transitions to the dielectric constant and is equal to the dielectric constant of the semiconductor in the absence of any excitation. The contribution of free electrons and holes, created by an optical excitation, enters the dielectric constant through the term $\chi_{\text{Drude}}(\omega)$, given by [3]:

$$\chi_{\text{Drude}}(\omega) = \frac{\mathrm{i}(Ne^2/m^*)\tau}{\omega(1 - \mathrm{i}\omega\tau)} = \frac{\mathrm{i}\omega_p^2\tau}{4\pi\omega(1 - \mathrm{i}\omega\tau)} \tag{2}$$

where N is the density of free electrons in the conduction band and holes in the valence band (the density of conduction electrons is equal to that of holes for the case of optical excitation because every excited electron leaves behind one hole in the valence band), m^* is a reduced effective mass for the free carriers, and τ is the average mean free time between collisions of free carriers with ions. The plasma frequency ω_p is the resonant frequency for collective excitations of the free carriers (plasmons). Setting $\chi_{\text{interband}}(\omega) = 0$ in this model gives the dielectric constant for a metal, in which the optical response is dominated by free carriers instead of by interband transitions.

In the modified Drude model, both the real part and the imaginary part of the dielectric constant are a function only of the free carrier density N. Because this

model assumes that $\chi_{\text{interband}}(\omega)$ is constant, it is valid only when changes in $\chi_{\text{interband}}(\omega)$ due to excitation are much smaller than the corresponding changes in $\chi_{\text{Drude}}(\omega)$. Under these circumstances, this model can be applied to interpret reflectivity measurements. It has been widely used in experiments involving free carrier densities up to 10^{20} cm^{-3} [17]. However, as we will see, for densities on the order of $10^{21} - 10^{22}$ cm^{-3}, which is roughly the excitation regime necessary to destabilize the lattice, changes in $\chi_{\text{interband}}(\omega)$ become too great to ignore, and the modified Drude model can no longer be applied.

19.2.2 Second-Harmonic Generation

Another optical probe used to study laser-induced structural change involves the nonlinear process of second-harmonic generation [18–20]. In this technique, a detector measures radiation at the second-harmonic frequency of the probe produced in the material. This type of measurement allows one to monitor changes in the second-order optical response of the material. In general, the optical response of a material is governed by the optical susceptibility χ. The linear response of a material to an optical field $E(\omega)$, involving processes such as reflection, transmission, and absorption, is given by the linear electric polarization

$$\boldsymbol{P}^{(1)}(\omega) = \overline{\overline{\chi}}^{(1)}(\omega) \cdot \boldsymbol{E}(\omega) \tag{3}$$

Similarly, the second-order response of a material to $\boldsymbol{E}(\omega)$ is given by the second-order electric polarization

$$\boldsymbol{P}^{(2)}(2\omega) = \overline{\overline{\overline{\chi}}}^{(2)}(2\omega = \omega + \omega) : \boldsymbol{E}(\omega)\,\boldsymbol{E}(\omega) \tag{4}$$

The second-order electric polarization, which is produced by an electric field oscillating with frequency ω, acts as a source which drives an electric field oscillating with frequency 2ω [21].

The reason for monitoring the second-order optical response in a laser-induced structural change experiment is that the second-order susceptibility $\chi^{(2)}$ reflects the symmetry of the system. For instance, in a material with inversion symmetry, $\chi^{(2)}$ remains unchanged by an inversion operation. The vectors $\boldsymbol{P}^{(2)}(2\omega)$ and $\boldsymbol{E}(\omega)$, however, change sign under inversion. Thus, an inversion operation on Eq. (4) produces

$$-\boldsymbol{P}^{(2)}(2\omega) = \overline{\overline{\overline{\chi}}}^{(2)}(2\omega = \omega + \omega) : [-\boldsymbol{E}(\omega)][-\boldsymbol{E}(\omega)] \tag{5}$$

implying that for a material with inversion symmetry (cf. Eqs. (4) and (5)),

$$\overline{\overline{\overline{\chi}}}^{(2)}(2\omega = \omega + \omega) = -\overline{\overline{\overline{\chi}}}^{(2)}(2\omega = \omega + \omega) = 0 \tag{6}$$

In other words, no second-harmonic radiation can be produced in a material with inversion symmetry. A III–V semiconductor such as GaAs does not have inversion

symmetry, so second-harmonic radiation can be produced in such a crystal. However, structural change resulting from an excitation by a pump pulse can change the crystal symmetry in such a way so that the material takes on inversion symmetry. A vanishing of the second-order susceptibility then serves to signal a change in the chemical bond structure.

A problem with the second-harmonic probe lies in the difficulty in interpreting the measurements – a drop in the detected second-harmonic radiation does not necessarily imply a drop in $\chi^{(2)}$. This complication arises because the second-harmonic radiation depends not only on $\chi^{(2)}$, but also on the linear susceptibility $\chi^{(1)}$ at both the fundamental and second-harmonic frequencies [22]. Any pump-induced changes in the linear reflectivity, the absorption depth, and the angle of refraction, all determined by $\chi^{(1)}$, will affect the detected second-harmonic radiation. If these changes induced in $\chi^{(1)}$ are small enough, then second-harmonic radiation measurements will reflect primarily the behavior of $\chi^{(2)}$. However, as will be shown Section 19.3, the changes in $\chi^{(1)}$ during femtosecond laser-induced structural change are actually quite large and cannot be ignored when analyzing second-harmonic generation results.

19.2.3 The Dielectric Constant – an Intrinsic Material Property

As described above, neither reflectivity nor second-harmonic probe yield unambiguous information on the behavior of the material. Interpretation of data taken using these probes is difficult and cannot be done without assumptions that are generally not valid in the regime of laser-induced structural changes. The difficulty in interpretation stems from the fact that reflectivity and second-harmonic radiation are not in themselves intrinsic material properties, but rather quantities that depend on a number of intrinsic material properties. To obtain clear, direct information on the response of the material to an excitation, one must therefore determine the effect of the excitation on an intrinsic material property such as the dielectric constant $\varepsilon = 1 + 4\pi\chi^{(1)}$.

19.2.3.1 Time-Resolved Measurements

To determine the real part and the imaginary part of the dielectric constant of a material at a certain frequency, one must have at least two independent pieces of information on the optical response of the material at that frequency. This information can take the form of the reflectivity of the material at that frequency for a particular polarization but at two different angles of incidence, or the reflectivity for a particular angle of incidence but at two different incident polarizations. Furthermore, if the dielectric constant is changing rapidly in time, as in the case of laser-induced structural change, the reflectivity measurements must occur on a timescale which is short compared with that over which the dielectric constant is changing.

More than one method exists for determining the time-dependent dielectric constant [23], but here we will focus on a technique that we used recently to study laser-induced structural changes in GaAs. We measured the reflectivity for light polarized in the plane of incidence with 70-fs probe pulses simultaneously at two different angles of incidence. Using the Fresnel formula for reflectivity as a function of dielectric constant and angle of incidence, we then converted the two simultaneous but independent reflectivity measurements into a real part and an imaginary part of the dielectric constant. By varying the relative time delay between a pump pulse, which induces the change in the dielectric constant, and the pair of probe pulses, we obtained the time evolution of the dielectric constant following the excitation.

19.2.3.2 Choosing the Angles of Incidence

To distinguish between the real and imaginary parts of the dielectric constant using this two-angle technique, one must choose angles of incidence which respond differently to changes in the dielectric constant [24]. Specifically, the two incident angles θ_1 and θ_2 must satisfy the condition

$$\frac{\partial R_p(\theta_1)/\partial \mathrm{Re}(\varepsilon)}{\partial R_p(\theta_1)/\partial \mathrm{Im}(\varepsilon)} \neq \frac{\partial R_p(\theta_2)/\partial \mathrm{Re}(\varepsilon)}{\partial R_p(\theta_2)/\partial \mathrm{Im}(\varepsilon)} \tag{7}$$

where $R_p(\theta)$ is the reflectivity at incident angle θ for light polarized in the plane of incidence. For pairs of angles of incidence less than roughly 45°, the ratios of the partial derivatives are almost the same, so that distinction between the real and imaginary parts of the dielectric constant is practically impossible. However, for pairs of larger incident angles, the partial derivative ratios do satisfy Eq. (7). Figure 19.3 illustrates the effect of a small change in the dielectric constant on the reflectivity for light polarized in the plane of incidence as a function of angle of incidence. Because the Brewster angle (the angle of minimum reflectivity) is the only angle at which the reflectivity is sensitive only to changes in the imaginary part, setting one of the two incident angles to the Brewster angle will assure that Eq. (7) is satisfied. In the experiment described below, we set one probe beam to be incident at Brewster angle (75.8°) and the other a few degrees away at 70.9°. This choice of angles, though optimized for small changes in the dielectric constant, satisfies Eq. (7) even for the large changes in the dielectric constant which we observe.

While reflectivity measurements at two carefully chosen incident angles are sufficient to extract the dielectric constant, additional measurement of the reflectivity at a third angle of incidence provides an important consistency check. The choice of the specific angle for this purpose is not critical. As a consistency check for our experiment, we measured the reflectivity at an incident angle of 45° under excitation conditions similar to those in the two-angle measurements. The measured 45° reflectivities show excellent agreement with 45° reflectivity values calculated using the dielectric constant extracted from our measurements at 75.8° and 70.9°.

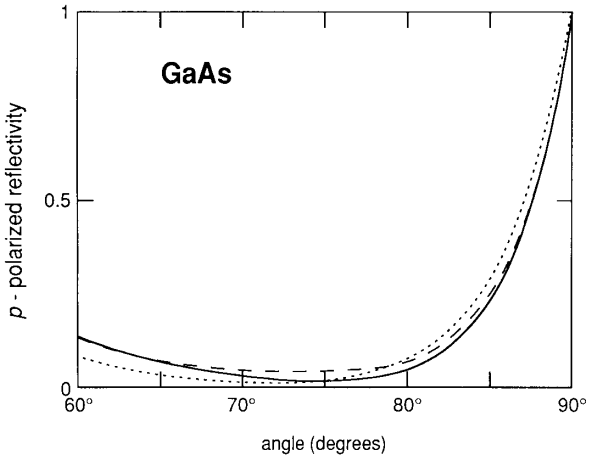

Figure 19.3 Effect of small changes in the dielectric constant on the angle dependence of the plane-polarized reflectivity of GaAs: —, no change in ε, -----, small change in $\mathrm{Re}(\varepsilon)$, — —, small change in $\mathrm{Im}(\varepsilon)$.

19.2.3.3 Three-Phase Model

Another important consideration in implementing this technique is the condition of the sample surface. In general, an oxide layer will form on the surface of a semiconductor exposed to air. The presence of this layer alters the reflectivity of the sample and must be taken into account when converting simultaneous reflectivity measurements to values for the dielectric constant. This effect can be included in the conversion by using a three-phase model of air–oxide–semiconductor for the system being studied [25]. This model assumes a sharp interface between the air and the oxide layer and between the oxide layer and the semiconductor and accounts for reflections from both interfaces. The effect of surface roughness on reflectivity is similar to that of an oxide layer, so with a modified effective thickness for the oxide layer in the calculation, the three-phase model can also account for surface roughness [25]. We obtained a value for the effective thickness of the oxide layer on the surface of our sample by measuring the incident angle dependence of the reflectivity in the absence of any excitation. With the known dielectric constant of GaAs [26] and a value of $\varepsilon = 4$ for the dielectric constant of the oxide layer [25], a fit of the three-phase model to the measured angle dependence yielded an effective oxide layer thickness of 42 Å.

19.3 Behavior of the Dielectric Constant in GaAs

In the remainder of this chapter we focus on our recent work on GaAs as a specific example of femtosecond laser-induced structural change. In this experiment we measure the dielectric constant at a probe wavelength of 570 nm (2.2 eV) at a series of time delays following excitation with a pump pulse at a wavelength of 635 nm (1.9 eV). The photon energy of the pump pulse is well above the band gap minimum of GaAs (1.4 eV), allowing excitation of a high density of free carriers through both linear and nonlinear absorption. The excitation conditions in this experiment are similar to those in other recent experiments on GaAs using the techniques described in Sections 19.2.1 and 19.2.2 [14–16]. However, the information contained in the dielectric constant measurements presented below provides important new insight into laser-induced structural changes as well as direct data on an intrinsic material property.

19.3.1 Experimental Setup

The pump and both probe beams are derived from the amplified output of a colliding-pulse mode-locked (CPM) laser, which produces a train of 100-fs pulses centered at 620 nm. Self-phase modulation in a single-mode fiber broadens the spectrum of the 620-nm pulses from about 5 nm to roughly 200 nm [27]. Following this spectral broadening, a beamsplitter splits the output from the fiber into two beams. One of the beams passes through a three-stage amplifier using the dye DCM to amplify a 20-nm spectral region centered at 635 nm while the other beam passes through a two-stage amplifier using the dye Rhodamine 6G to amplify a 10-nm region centered at 570 nm. Both amplifiers are pumped by a frequency-doubled, 10-Hz Nd:YAG laser. A separate grating pair compresses the amplified pulses in each of the two beams to about 70fs (full width at half-maximum; FWHM). Another beamsplitter then splits the 570-nm beam into the two probe pulses.

All three beams are polarized in the plane of incidence and are focused to the same spot on the sample, which is an insulating (110) GaAs wafer (Cr doped, $\rho > 7 \times 10^7$ Ω cm) in air. To monitor a uniformly excited region, the two probe beams, incident at 75.8° and at 70.9° from the surface normal, are focused more tightly than the pump beam, incident at 63° (see Fig. 19.4). The probed surface area is about 16 times smaller than the 0.01-mm^2 focal area of the pump beam on the sample. Uniform excitation in the probed region is further assured by the smaller penetration depth of the probe beams ($\leq$170 nm, depending on the strength of the excitation) compared with that of the pump beam (270 nm).

To measure the time dependence of the dielectric constant, we vary the time delay between the pump and the probe pulses. This is achieved by changing the difference in optical path lengths to the sample between pump and probe. The zero in time is defined by maximum temporal overlap of pump and probe at the sample. We determine this zero in time by maximizing the nonlinear sum-frequency signal produced by each pair of beams as we vary the optical path lengths. At each pump–probe time

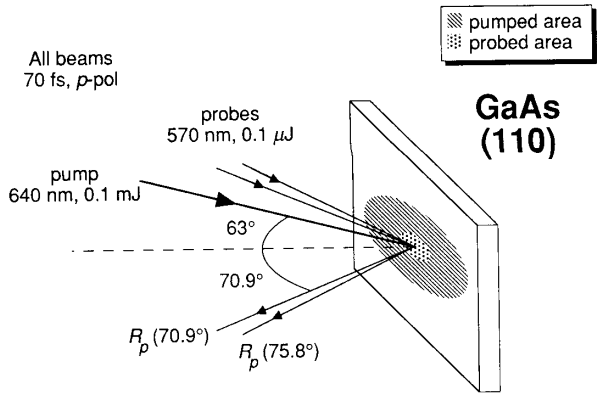

Figure 19.4 Probing geometry; *p*-pol,, plane-polarized.

delay, the collected data span a range of pump-pulse fluence from 0 to 3.2 kJ m^{-2}. The fluence of each probe beam is kept below 0.1 kJ m^{-2} so as not to produce any detectable changes in the dielectric constant to within our experimental resolution. Since the excitation can permanently alter the material, the sample is translated during data collection so that each data point is obtained at a different spot on the sample.

19.3.2 Experimental Results

Figure 19.5 summarizes the experimentally measured dielectric constant of GaAs at 2.2 eV following femtosecond laser pulse excitation. The four graphs in Fig. 19.5(a) show the real part (•) and the imaginary part (o) of the dielectric constant plotted as a function of time delay for four different pump-pulse fluences. The behavior of the dielectric constant is particularly revealing when viewed as a function of pump pulse fluence at fixed time delay, as shown in Fig. 19.5(b). In all four of these graphs, the imaginary part of the dielectric constant $\mathrm{Im}(\varepsilon)$ rises from an initial value close to 2 to a peak of roughly 60. Coincident with the peak in $\mathrm{Im}(\varepsilon)$ is a drop through zero in the real part of the dielectric constant, $\mathrm{Re}(\varepsilon)$. The peak in $\mathrm{Im}(\varepsilon)$ and zero-crossing of $\mathrm{Re}(\varepsilon)$ occur earlier in time at higher pump fluences than at lower ones. This fact is highlighted in Fig. 19.6, which shows a plot of the time delay at which this feature occurs as a function of pump fluence. The lowest fluence at which we still observe a peak and zero-crossing is 0.8 kJ m^{-2}. This is slightly below the 1.0 kJ m^{-2} threshold for permanent visible damage which we determined by correlating the incident energy of a pump pulse with the size of the damage spot it produces on the sample.

The behavior of the dielectric constant seen in Fig. 19.5 is characteristic of an absorption peak coming into resonance with the probe frequency. In general, $\mathrm{Re}(\varepsilon)$ is positive for frequencies below and negative for frequencies above the resonant frequency of an absorption peak. The direction of the zero-crossing of $\mathrm{Re}(\varepsilon)$ in

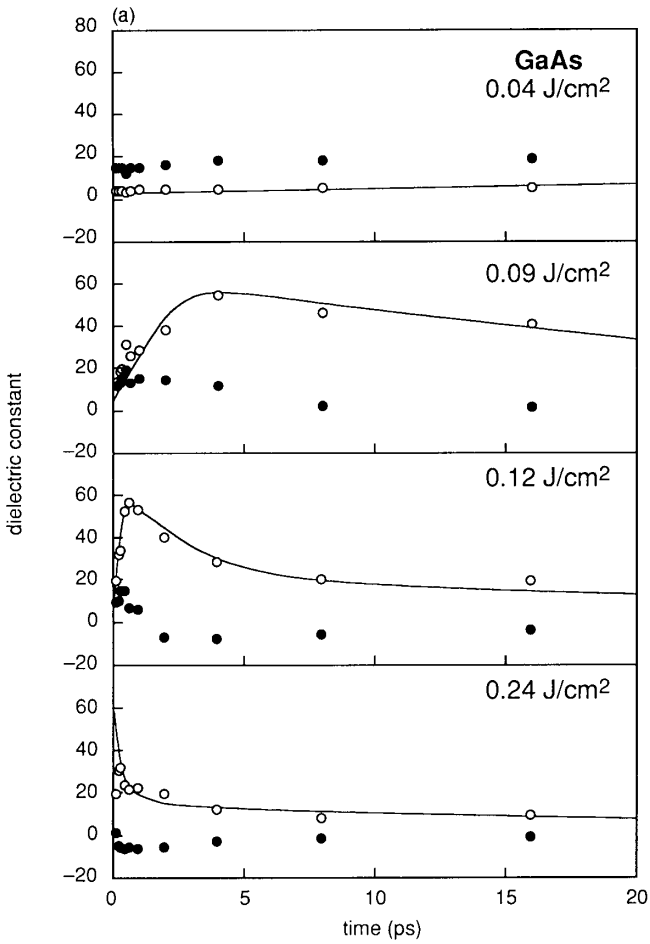

Figure 19.5(a) For caption, see following page.

Fig. 19.5 thus implies that the resonant frequency of a major absorption peak, initially above the probe frequency of 2.2 eV, drops down through the probe frequency as a result of the pump pulse excitation. Figure 19.6 suggests that the strength of the excitation determines the rate and extent of the drop: the higher the pump fluence, the faster and further the drop. For pump fluences less than 0.8 kJ m^{-2}, the resonant frequency of this absorption peak does not decrease all the way to the probe frequency.

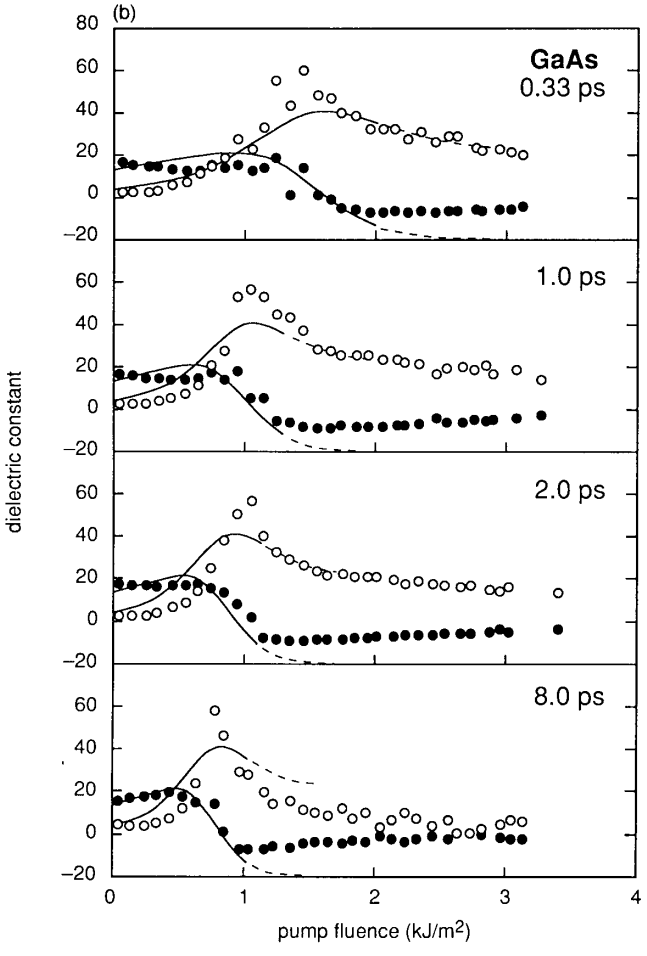

Figure 19.5 (a, previous page) Dielectric constant at 2.2 eV versus pump-probe time delay for four different pump fluences. The curves are drawn in to guide the eye. (b) Dielectric constant at 2.2 eV versus pump fluence for four different pump-probe time delays. The curves are calculated using a single-oscillator model for the dielectric constant. •, Re(ε); ○, Im(ε); p-pol.

19.3.3 Interpretation of Results

The distinct behavior of the dielectric constant presented in Section 19.3.2 is somewhat surprising. While the system being studied is extremely complex, the graphs in Fig. 19.5 are all dominated by one particularly striking feature – an absorption peak coming into resonance with the probe frequency. In fact, all the data in Fig. 19.5(b) can be made to overlap by simply rescaling the fluence axis of each graph. The simplicity of the results suggests that a simple model may account for the behavior of the dielectric constant.

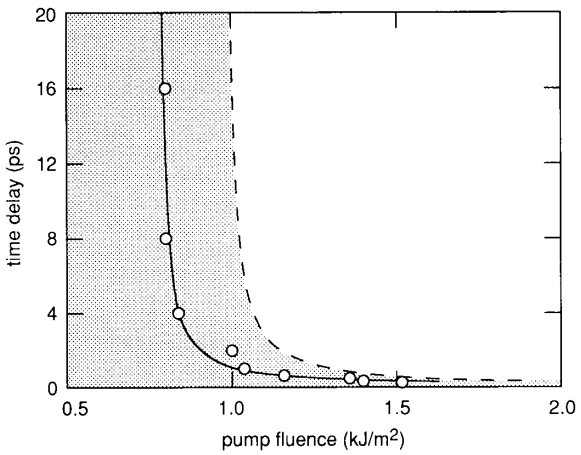

Figure 19.6 Pump-probe time delays at which $\mathrm{Im}(\varepsilon)$ is maximal and $\mathrm{Re}(\varepsilon) = 0$ for different pump fluences. The solid line is a fit of Eq. (9) to the data with $\omega_0(\phi, t) = \omega_{\mathrm{probe}}$; the broken line corresponds to the semiconductor-metal transition where $\omega_0(\phi, t) = \omega_{\mathrm{cr}}$. The single-oscillator model is valid only in the stippled region, where GaAs is a semiconductor.

19.3.3.1 Single-Oscillator Model for the Semiconductor Dielectric Function

To identify the absorption peak in the data, we should look at the main features of the dielectric function in semiconductors. The dielectric function of GaAs is typical of most direct-gap semiconductors and is shown by the solid curves in Fig. 19.7 [26].

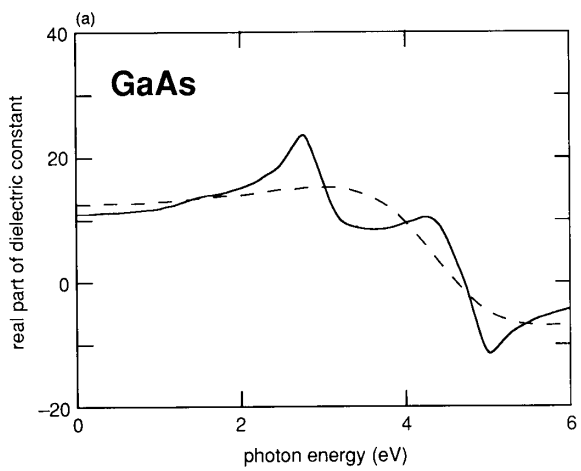

Figure 19.7(a) For caption, see following page.

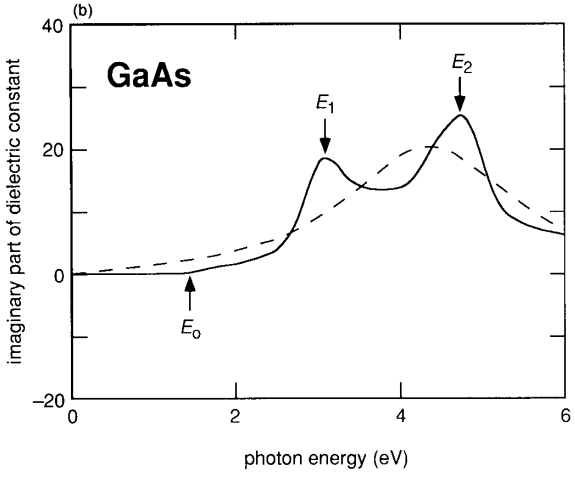

Figure 19.7 (a, previous page) $\mathrm{Re}(\varepsilon)$ and (b) $\mathrm{Im}(\varepsilon)$ for GaAs as a function of photon energy in the absence of any excitation (solid curves) [26]. Also shown is a fit (broken curves) of the single-oscillator model given by Eq. (8) to the dielectric function. E_0 corresponds to the minimum band gap, below which there is no absorption, while E_1 and E_2 label the two main absorption peaks.

The first feature to notice is the point labeled E_0 in Fig. 19.7(b), which corresponds to the minimum in the band gap. For photon energies above this point, the dielectric function is dominated by direct interband transitions, or transitions at the same k-vector between valence and conduction bands. No interband absorption can occur for photon energies below this point, so $\mathrm{Im}(\varepsilon)$ is zero in that region. The two absorption peaks E_1 and E_2 result from regions in the band structure in which the valence band is parallel to the conduction band, leading to a large joint density of states for direct interband transitions [28]. The E_2 peak is the stronger of the two, and its center frequency, 4.75 eV for GaAs [29], gives roughly the average bonding–antibonding splitting of the material [2].

The dielectric function of GaAs can be approximated by that of a single harmonic oscillator with a resonant frequency equal to the average bonding–antibonding splitting [28]. The single-oscillator dielectric function is given by

$$\varepsilon(\omega) = 1 - \frac{\omega_p^2}{\omega^2 - \omega_0^2 + i\dfrac{\omega}{\tau}} \tag{8}$$

where the plasma frequency ω_p corresponds to the oscillator strength, ω_0 is the resonant frequency of the oscillator, and $1/\tau$ the width of the resonance. A fit of Eq. (8) to the actual dielectric function of GaAs (see Fig. 19.7) yields $\omega_p = 15.2$ eV, $\omega_0 = 4.55$ eV, and $\tau = 0.39\ \mathrm{eV}^{-1}$. The value of ω_p extracted from the fit closely matches the 15.5-eV plasma frequency calculated using the total valence electron density

of GaAs [30]. Note also that the value obtained for ω_0 agrees with the average bonding–antibonding splitting of GaAs, given roughly by the 4.75-eV location of the E_2 absorption peak of GaAs. Thus, while the single-oscillator model smooths out the features of the real dielectric function, it captures the essential physics.

The model in Eq. (8) provides a simple identification of the absorption peak in the data in Fig. 19.5 as the single-oscillator resonant frequency ω_0. With this identification, the data imply that ω_0 depends on fluence ϕ and time delay t, $\omega_0 = \omega_0(\phi, t)$; it starts off at an initial value $\omega_0(0, 0) = 4.55$ eV and decreases as a result of the pump pulse excitation. The magnitude and rate of this drop depend on the strength of the excitation. The laser-induced drop in the resonant frequency can be described phenomenologically by

$$\omega_0(\phi, t) = 4.55 \text{ eV} - C\left(1 + \frac{T}{t}\right)^{-1} \phi \tag{9}$$

where C and T are constants which can be determined from a fit to the data in Fig. 19.6 since these points indicate the fluences and times at which $\omega_0(\phi, t) = \omega_{\text{probe}} = 2.2$ eV. Substituting 2.2 eV into the left-hand side of Eq. (8) and fitting the resulting expression to the data points in Fig. 19.6 yields $C = 3.0$ eV kJ^{-1} m^2 and $T = 0.34$ ps. Substituting Eq. (9) into Eq. (8) produces an expression for the dielectric function of GaAs as a function of fluence and time following excitation with the pump pulse. This expression is represented by the curves in Fig. 19.5(b), which are plotted up to the fluence at which the resonant frequency reaches zero, $\omega_0(\phi, t) = 0$.

19.3.3.2 Semiconductor–Metal Transition

The single-oscillator model in Eq. (8) approximates the dielectric constant for a semiconductor, whose optical response is dominated by interband transitions. However, if the average bonding–antibonding splitting decreases so far that the minimum of the conduction band drops below the maximum of the valence band, then free charge carrier contributions to the dielectric constant, dominated by intraband transitions, will start to become important as the material takes on a metallic character. In terms of the bonding picture presented in Figs 19.1 and 19.2, this transition from semiconductor to metal occurs when the average bonding–antibonding splitting, characterizing the strength of the covalent bonding, becomes smaller than the width of the energy bands, characterizing the strength of the metallic bonding. Figure 19.8 illustrates this pump pulse-induced transition schematically.

At what time delay does the conduction band minimum just reach the valence band maximum? This overlap point corresponds to a critical value of the average bonding–antibonding splitting, ω_{cr}. Since the rate of decrease of the average bonding–antibonding splitting increases with excitation strength, the time delay t at which $\omega_0(\phi, t) = \omega_{\text{cr}}$ will decrease with increasing pump fluence ϕ. We can estimate the value of ω_{cr} by assuming that the minimum value of ϕ for which $\omega_0(\phi, t)$ reaches ω_{cr} corresponds to the 1.0 kJ m^{-2} threshold fluence for irreversible damage of the

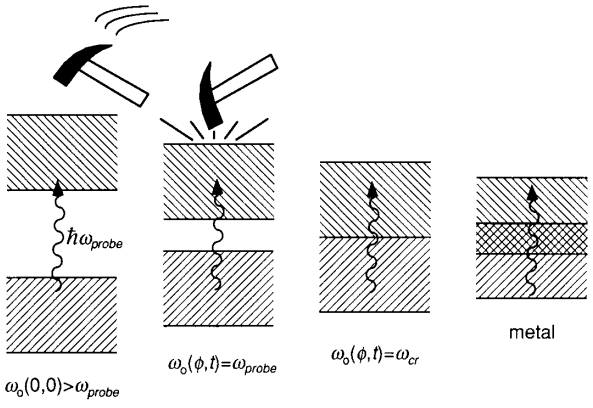

Figure 19.8 Schematic illustration of semiconductor–metal transition induced by femtosecond laser pulse excitation (represented by initial hammer blow).

material. At this fluence, then, the average bonding–antibonding splitting decreases just far enough so that at infinite time $\omega_0(1.0\ \text{kJ m}^{-2}, \infty) = \omega_{cr}$. Using these values for ϕ and t in Eq. (9) yields a value of approximately 1.6 eV for ω_{cr}. It should be emphasized that this value is based on the single-oscillator model and is therefore limited by the accuracy of the model.

Substituting $\omega_{cr} = 1.6$ eV for the left-hand side of Eq. (9) produces a curve for the time delay at which the semiconductor–metal transition occurs as a function of pump fluence, shown as the broken curve in Fig. 19.6. The stippled region of the graph to the left of the broken curve corresponds to $\omega_0(\phi, t) > \omega_{cr}$, for which the material is still a semiconductor. The white region to the right of the broken curve corresponds to $\omega_0(\phi, t) < \omega_{cr}$, for which the material is metallic. For fluences greater than 2.0 kJ m^{-2}, the transition takes place in under 1 ps. However, for pump fluences less than 1.0 kJ m^{-2}, the excitation is not strong enough to cause this transition at all. Once the material becomes metallic, the single-oscillator model described by Eq. (8) is no longer a valid approximation for the dielectric constant. This can be seen in Fig. 19.5(b), in which the calculated semiconductor–metal transition point is marked in each graph by a transition from solid line to broken line in the single-oscillator model curves. Note that the curves do indeed start to deviate from the experimental data once they become broken.

19.4 Discussion of Band Gap Collapse

The experimental results presented in Section 19.3 indicate that sudden excitation of a high density of free carriers by a femtosecond laser pulse directly leads to a collapse of the band gap, signaled by a drop in the average bonding–antibonding splitting. How does an electronic excitation cause such a collapse? Fundamentally, the band

structure of a solid is a result of Coulomb interactions among the component nuclei and electrons. Any changes in the strength of the Coulomb interactions between atoms will therefore affect the average bonding-antibonding splitting. The strength of the interatomic interactions can be modified both by changes in the effective range of Coulomb forces through screening by free carriers and by changes in the relative positions of the interacting atoms themselves.

19.4.1 Electronic Screening

The creation of free electrons and holes by femtosecond laser pulse excitation introduces into the system a sizable population of mobile charge carriers that will reduce the effective range of Coulomb forces in the material. In other words, a positive ion will attract a negative charge cloud that in turn screens out to a certain extent the electric field of the ion [3]. This electronic screening thus reduces the interatomic interaction strength, thereby diminishing the average bonding-antibonding splitting. The extent to which electronic screening decreases the average bonding-antibonding splitting will depend on the density of free carriers; a higher density allows more efficient screening, causing a bigger decrease in the splitting.

In our experiment, the excited carrier densities are greater than 10^{21} cm^{-3}. At these densities the decrease in the band gap due to electronic screening can be a sizable fraction of the gap [17, 31]. A precise value for the size of this effect is hard to calculate, in part because the exact density of excited free carriers is not known. However, we can assume that electronic screening will be strongest immediately following the pump pulse because that is when the free carrier density is highest. As this excited population decreases through recombination and diffusion processes, the effect of electronic screening on the average bonding-antibonding splitting must also decrease. In contrast, the experimental data show that the effect of the excitation on the average bonding-antibonding splitting continues to increase for picoseconds despite the 70 fs width of the excitation pulse. Thus, while electronic screening may account for some of the initial drop in the average bonding-antibonding splitting, it cannot account for the entire effect evident in the data.

19.4.2 Structural Change

Changes in the lattice structure will also have a strong effect on the band structure. Band gap collapse is known to occur as a result of structural transformations induced by high pressure or by thermal melting [32-34]. A 10% change in the bond length is enough to cause a semiconductor-metal transition [32]. Structural change of this magnitude is easily attainable on the timescale of the drop in the average bonding-antibonding splitting described in Section 19.3. To move 10% of the bond length of GaAs in 1 ps, an ion need only move at a speed of 25 ms^{-1}.

To understand how the femtosecond laser pulse excitation can destabilize the lattice and directly lead to structural change, we should look again at the mechanism

for covalent bonding. As discussed in Section 19.1.1, a covalent bond is energetically favorable when the two electrons that make up the bond are in the ground state. If one of the electrons is excited to the antibonding level, then the total energy of the system is no longer lower than that of two isolated atoms. Under this type of excitation, the component atoms will move away from each other, as is seen in the case of photodissociation of molecules [35]. The situation is much more complicated in a covalent solid where there are on the order of 10^{23} atoms cm^{-3}, but we can expect a similar kind of bond instability if enough electrons are excited from bonding valence-band states to antibonding conduction-band states. Once this lattice instability is set up by the initial excitation, the lattice structure will continue to evolve toward a lower-energy configuration even after the pump pulse is gone, in agreement with the evolution of the data presented in Section 19.3.

19.5 Conclusion

Although the field of laser-induced structural change in semiconductors has been an important topic of research since the 1970s, it continues to generate new interest with each result. The advent of femtosecond laser technology, in particular, opened a new and growing list of questions to be answered. What, for instance, is the nature of electron–lattice interactions when a significant fraction of the valence electrons have been excited to the conduction band? To what new configuration does the lattice evolve once the tetragonally coordinated covalent structure becomes unstable? As the results presented here show, these questions strike at the very core of the connection between chemical bonds and energy bands.

To answer such questions, it will be necessary to characterize fully the behavior of the band structure following intense femtosecond laser pulse excitation. This chapter represents a first step in this characterization. As we add to current experimental information on the intrinsic material properties of laser-excited materials, theoretical calculations will play an increasingly important role in the field. Progress in the study of laser-induced lattice instability and structural change will lead to a more complete picture of the cohesion of solids.

Acknowledgements

We appreciate many useful discussions with Professors N. Bloembergen, H. Ehrenreich, and E. Kaxiras. E. Glezer gratefully acknowleges a Fannie and John Hertz Fellowship. This work was supported by contract numbers ONR N00014-89-J-1023 and NSF DMR 89-20490.

Final version received: 7th October 1993.

References

[1] E. I. Shtyrkov, I. B. Khaibullin, M. M. Zaripov, M. F. Galyatudinov and R. M. Bayazitov, *Sov. Phys. – Semicond.* **1976,** *9,* 1309.

[2] W. A. Harrison, *Electronic Structure and the Properties of Solids: The Physics of the Chemical Bond,* Dover, New York, **1989.**

[3] N. W. Ashcroft, N. D. Mermin, *Solid State Physics,* Saunders College, Philadelphia, **1976.**

[4] R. F. Wood, C. W. White, R. T. Young, *Semiconductors and Semimetals,* Vol. 23, Academic Press, New York, **1984.**

[5] H. Kurz, N. Bloembergen in *Energy Beam-Solid Interactions and Transient Thermal Processing* (Ed.: D. K. Biegelsen, G. A. Rozgonyi, C. V. Shank), Materials Research Society, Pittsburgh, **1985,** p. 3.

[6] A. M. Malvezzi in *Excited-State Spectroscopy in Solids* (Ed.: U. M. Grassano, N. Terzi), North-Holland Physics, Amsterdam, **1987,** p. 335.

[7] J. A. Van Vechten, R. Tsu, F. W. Saris, *Phys. Lett. A* **1979,** *74,* 422.

[8] J. A. Van Vechten in *Semiconductors Probed by Ultrafast Laser Spectroscopy* (Ed.: R. R. Alfano), Academic Press, San Diego, **1984,** p. 95.

[9] J. A. Kash, J. C. Tsang, J. M. Hvam, *Phys. Rev. Lett.* **1985,** *54,* 2151.

[10] C. V. Shank, R. Yen, C. Hirlimann, *Phys Rev Lett* **1983,** *51,* 900.

[11] D. H. Reitze, T. R. Zhang, W. M. Wood, M. C. Downer, *J. Opt. Soc. Am. B* **1990,** *7,* 84.

[12] M. C. Downer, R. L. Fork, C. V. Shank, *J. Opt. Soc. Am. B* **1985,** *2,* 595.

[13] H. W. K. Tom, G. D. Aumiller, C. H. Brito-Cruz, *Phys. Rev. Lett.* **1988,** *60,* 1438.

[14] S. V. Govorkov, I. L. Shumay, W. Rudolph, T. Schroeder, *Opt. Lett.* **1991,** *16,* 1013.

[15] K. Sokolowski-Tinten, H. Schulz, J. Bialkowski, D. von der Linde, *Appl. Phys. A* **1991,** *53,* 227.

[16] P. N. Saeta, J. Wang, Y. Siegal, N. Bloembergen, E. Mazur, *Phys. Rev. Lett.* **1991,** *67,* 1023.

[17] H. M. van Driel, *Phys. Rev. B* **1987,** *35,* 8166.

[18] S. A. Akhmanov, N. I. Koroteev, G. A. Paitan, I. L. Shumay, M. V. Galjautdinov, I. B. Khaibullin, E. I. Shtyrkov, *Opt. Commun.* **1983,** *47,* 202.

[19] S. A. Akhmanov, V. I. Emel'yanov, N. I. Koroteev, V. N. Seminogov, *Sov. Phys. Usp.* **1985,** *28,* 1084.

[20] J. M. Liu, A. M. Malvezzi, N. Bloembergen in *Energy Beam-Solid Interactions and Transient Thermal Processing* (Ed.: D. K. Biegelsen, G. A. Rozgonyi, C. V. Shank), Materials Research Society, Pittsburgh, **1985,** p. 137.

[21] Y. R. Shen, *The Principles of Nonlinear Optics,* John Wiley, New York, **1984.**

[22] Y. R. Shen, *The Principles of Nonlinear Optics,* John Wiley, New York, **1984,** p. 75.

[23] J. I. Dadap, H. R. Choo, X. F. Hu, Q. Deng, M. C. Downer in *Ultrafast Pulse Generation and Spectroscopy* (Ed.: T. R. Gosnell, A. J. Taylor, K. A. Nelson, M. C. Downer), SPIE Proc., **1993,** p. 1861.

[24] D. L. Greenaway, G. Harbeke, *Optical Properties and Band Structure of Semiconductors,* Pergamon Press, Oxford, **1968.**

[25] R. F. Potter in *Optical Properties of Solids* (Ed.: S. Nudelman, S. S. Mitra), Plenum Press, New York, **1969,** Chapter 16.

[26] E. D. Palik in *Handbook of Optical Constants of Solids* (Ed.: E. D. Palik), Academic Press, New York, **1985,** p. 434.

[27] K. Wang, Y. Siegal, C. Z. Lü, E. Mazur, *Opt. Commun.* **1992,** *91,* 77.

[28] M. L. Cohen, J. R. Chelikowsky, *Electronic Structure and Optical Properties of Semiconductors,* Springer-Verlag, Berlin, **1988.**
[29] D. E. Aspnes, G. P. Schwartz, G. J. Gualtieri, A. A. Studna, B. Schwartz, *J. Electrochem. Soc.* **1981,** *128,* 590.
[30] H. R. Philipp, H. Ehrenreich, *Phys. Rev.* **1963,** *129,* 1550.
[31] H. Kalt, M. Rinker, *Phys. Rev. B* **1992,** *45,* 1139.
[32] S. Froyen, M. L. Cohen, *Phys. Rev. B* **1983,** *28,* 3258.
[33] V. M. Glazov, S. N. Chizhevskaya, N. N. Glagoleva, *Liquid Semiconductors,* Plenum, New York, **1969.**
[34] W. Jank, J. Hafner, *J. Non-Crystalline Solids* **1989,** *114,* 16.
[35] A. H. Zewail, *Science* **1988,** *242,* 1645.